

Cite this article as: Cao Hui, Xu Hanzong, Li Haipeng, et al. Effect of Grain Size on Nano-scratching Behavior of Polycrystalline γ -TiAl Alloy via Molecular Dynamics Simulation[J]. Rare Metal Materials and Engineering, 2025, 54(03): 569-580. DOI: <https://doi.org/10.12442/j.issn.1002-185X.20240420>.

ARTICLE

Effect of Grain Size on Nano-scratching Behavior of Polycrystalline γ -TiAl Alloy via Molecular Dynamics Simulation

Cao Hui^{1,2}, Xu Hanzong¹, Li Haipeng³, Li Haiyan^{1,2}, Chen Tao⁴, Feng Ruicheng^{1,2}

¹School of Mechanical and Electrical Engineering, Lanzhou University of Technology, Lanzhou 730050, China; ²Engineering Research Center of Nonferrous Metallurgy's New Equipment, Ministry of Education, Lanzhou University of Technology, Lanzhou 730050, China; ³Yunnan Wenshan Aluminum Co., Ltd, Wenshan 663000, China; ⁴School of Mechanical Engineering and Rail Transit, Changzhou University, Changzhou 213164, China

Abstract: The scratching mechanism of polycrystalline γ -TiAl alloy was investigated at the atomic scale using the molecular dynamics method, with a focus on the influence of different grain sizes. The analysis encompassed tribological characteristics, scratch morphology, subsurface defect distribution, temperature variations, and stress states during the scratching process. The findings indicate that the scratch force, number of recovered atoms, and pile-up height exhibit abrupt changes when the critical size is 9.41 nm due to the influence of the inverse Hall-Petch effect. Variations in the number of grain boundaries and randomness of grain orientation result in different accumulation patterns on the scratch surface. Notably, single crystal materials and those with 3.73 nm in grain size display more regular surface morphology. Furthermore, smaller grain size leads to an increase in average coefficient of friction, removed atoms number, and wear rate. While it also causes higher temperatures with a larger range of distributions. Due to the barrier effect of grain boundaries, smaller grains exhibit reduced microscopic defects. Additionally, average von Mises stress and hydrostatic compressive stress at the indenter tip decrease as grain size decreases owing to grain boundary obstruction.

Key words: grain size; nano-scratching; surface generation; subsurface defect; polycrystalline γ -TiAl alloy

1 Introduction

As a newly developed structural metal material in the aerospace industry, γ -TiAl alloy possesses several advantages including low density, extreme temperature resistance, high specific strength, creep resistance, and antioxidant properties. It is considered as a significant alternative to Ti alloys and Ni-based elevated-temperature alloys for aero-engine applications and has a wide range of potential application. However, its low thermal conductivity, room-temperature brittleness, and machining adhesion restrict its machinability and practical application^[1-2]. The ultra-precision machining properties of TiAl alloy can be effectively enhanced by controlling its microstructure^[3]. Among them, refining the grain size to enhance material strength and mechanical properties has become a hot topic. Numerous scholars have achieved grain

refinement by introducing appropriate amounts of elements such as B and Cr^[4-5], as well as methods such as ultrasonic shot peening^[6], ultrasonic vibration treatment^[7-8], and cyclic air-cooling heat treatment^[9]. It is well known that at the microscale and nanoscale, the inverse Hall-Petch (H-P) effect may occur, which shows that the yield strength increases with the decrease in the average grain size, but when the grain is refined to the critical size, the strength and ductility of the material decrease^[10-11]. Numerous scholars have conducted relevant research on determining the critical grain size and its effect on material properties through experimental and numerical simulation methods combined with various material property testing methods.

Ding et al^[12] conducted uniaxial tensile simulations of polycrystalline γ -TiAl alloy using the molecular dynamics (MD) method and analyzed the effects of grain size and

Received date: July 12, 2024

Foundation item: National Natural Science Foundation of China (52065036, 52365018); Natural Science Foundation of Gansu (23JRRA760); Hongliu Outstanding Youth Foundation of Lanzhou University of Technology; China Postdoctoral Science Foundation (2023M733583)

Corresponding author: Feng Ruicheng, Ph. D., Professor, School of Mechanical and Electrical Engineering, Lanzhou University of Technology, Lanzhou 730050, P. R. China, Tel: 0086-931-5135199, E-mail: postfeng@lut.edu.cn

Copyright © 2025, Northwest Institute for Nonferrous Metal Research. Published by Science Press. All rights reserved.

temperature on its micro-deformation mechanism. The results indicate that when the grain size is less than 8 nm, the yield stress of material follows the inverse H-P effect, and the material exhibits a plastic deformation mode characterized by grain boundary migration and grain rotation. Conversely, when the grain size exceeds 8 nm, the sensitivity of yield stress to grain size decreases, with dislocation slip and deformation twins gradually dominating the plastic deformation process. Cao et al^[13] conducted MD simulations to investigate nano-indentation on polycrystalline γ -TiAl alloys. They concluded that the relationship between grain size and hardness follows the H-P relationship when the critical grain size is less than 9.9 nm. Additionally, they observed that the grain boundary lattice structure effectively inhibits the diffusion of internal stresses and indentation defects. Liu et al^[14] systematically investigated the tensile properties, tensile fracture behavior, and deformation mechanism of Ti-45.5Al-4Cr-2.5Nb master alloy, continuous casting alloy (C. C.), and heat-treated alloys by experiments. They discovered that the interlayer spacing of B2+ γ coupled structures in the pristine grains in C.C. alloy is significantly refined after annealing treatment at a high temperature of 1250 °C for 2 h. The uniform and fine microstructure effectively mitigates the tendency of stress concentration during the deformation process, which in turn alleviates the formation of micro-cracks in the coarse coupled structures and which further enhances the tensile properties of TiAl-based alloys at room temperature. Additionally, a large number of Shockley incomplete dislocations and laminations generated in the γ -phase are observed by transmission electron microscope. Cao et al^[15] employed supersonic fine particle bombardment to atomically simulate the surface grain refinement treatment of γ -TiAl alloy with varying grain sizes. The findings indicate that the refining effect is more pronounced with smaller grain sizes. This can be attributed to the fact that a smaller grain size results in larger interfacial areas between neighboring grains, thereby promoting dislocation reactions and annihilation at these interfaces. As a result, there is an increase in the number of active sites required for grain nucleation.

Whereas the methods for evaluating the overall mechanical properties of grain-refined materials after different process treatments have garnered attention from numerous scholars, it is equally essential to investigate the damage mechanisms and tribological behavior on the surface of γ -TiAl alloy materials. In comparison to single-loading methods, such as tensile and indentation, nano-scratching serves as a high-resolution approach for characterizing the tribological properties of materials as well as an atomic-level material removal method. It can provide valuable information such as acoustic emission signals, residual depths, coefficient of friction (COF), brittle-plastic failure points, and nano-channel preparation^[16-18]. In addition, the MD simulation of nano-scratches enables real-time observation of microscopic defect evolution and atomic flow processes that cannot be observed in experiments. This efficient and low-cost numerical simulation approach effectively provides theoretical support for experiments and

has received widespread attention in the academic community. Qi et al^[19] conducted a simulation to investigate the influence of microstructure on the nano-scratching process of nano-crystalline CoCrFeMnNi high entropy alloy. The findings revealed that polycrystalline materials exhibit higher COF than single-crystal materials and that as the grain size decreases, the stress concentration area increases. Doan et al^[20] conducted simulations on the mechanical behavior of CuAlNi nano-crystalline surface scratches with varying grain sizes. Through analysis of the simulation results regarding plastic deformation, microstructure and dislocations, and pile-up morphology, they concluded that the hindrance of strain and stress diffusion is attributed to the grain boundaries. They also highlighted the significance of slipping and torsion at the boundaries, as well as fusion of the grains, in the deformation process. Furthermore, it was observed that polycrystalline alloys exhibited a higher wear rate than single crystals. On a different note, Cha et al^[21] investigated dislocation motion and wear response in columnar nano-crystalline Ni materials. Their findings revealed that the COF decreased with an increase in grain size when comparing different spherical indenter sizes and effects of grain size on material frictional properties.

Currently, some scholars focus on the study of γ -TiAl alloy nano-scratching. Xie et al^[22] investigated the temperature-induced nano-scratch response of single-crystal γ -TiAl alloys using the MD method. The results indicated that an increase in temperature resulted in weakening of surface friction, normal force, and COF. Additionally, high temperature promoted the degree of amorphization and inhibited the movement of dislocations. Xu et al^[23] conducted numerical simulations of conical indenter tip scratches on the surface of γ -TiAl alloy nanowires in six different crystal orientations. They discovered that the evolution of microscopic defects within the workpiece is significantly influenced by the crystal orientation, leading to substantial dislocation motion-induced shear deformation and tool removal by extrusion. These factors play a crucial role in determining the shape of the varied surface pile-up and the overall deformation degree of the workpiece. Niu et al^[24] conducted an investigation on the reciprocating friction process of TiAl alloy with the γ/α_2 duplex structure. The elastic properties of the atoms lead to the formation of wear marks with a certain slope when the workpiece reaches the compacted state after reciprocating friction. Furthermore, the results indicate that the transition of face-centered cubic (fcc) to hexagonal close-packed (hcp) atoms occurs in conjunction with the creation and destruction of dislocations.

In summary, considering the single method for evaluating the mechanical mechanism and surface properties of polycrystalline materials, the current research on the scratching properties of γ -TiAl alloy surfaces mainly focuses on single-crystal and duplex structures. There are relatively few reports on the study of the mechanical mechanism of polycrystalline γ -TiAl alloys using the nano-scratching method from an atomic point of view. The existence of grain size

and grain boundaries is essential factors that cannot be ignored in the processing of actual materials. Therefore, this research establishes a MD model of polycrystalline γ -TiAl alloy, selects a conical diamond indenter tip to adopt the mode of first pressing and then scratching, simulates the surface nano-scratching behavior under different grain sizes, and comprehensively elucidates the surface scratching mechanism from multiple perspectives. The findings provide valuable reference data for the wide application of γ -TiAl alloys.

2 Models and Methods

2.1 Polycrystalline γ -TiAl scratching model in MD

In this study, a large-scale atomic-molecular parallel simulation (Lammps)^[25] was utilized to conduct simulations of the scratching process to obtain initial simulation data. As an illustration, Fig. 1a shows the nano-scratch model of polycrystalline γ -TiAl alloy with 36 grains. The workpiece has dimensions of 42 nm×25 nm×15 nm and is rectangular in shape. It is divided into three regions: the Newtonian layer, the thermostat layer, and the boundary layer. Material deformation occurs in the Newtonian layer, while the thermostat layer is maintained at 293 K for heat dissipation, and the boundary layer serves a fixed role. Different grains are depicted in different colors to represent polycrystalline materials. Additionally, a diamond tool with a tip radius of 6 nm is chosen and set as a rigid body with an initial position of 1 nm from the surface of the workpiece. The entire simulation

process consists of an indentation phase and a scratching phase. The scratching phase commences with an energy minimization process followed by relaxation for 100 ps to achieve an equilibrium state. Both relaxation and machining processes are conducted under the canonical ensemble and the micro-canonical ensemble, respectively. This equilibrium system is considered as an isolated state where only kinetic and potential energy conversions occur.

Fig. 1b depicts a top view of the workpiece, where grain boundaries and grains are colored in gray and green, respectively, and the common neighbor analysis (CNA) was used to precisely illustrate the distribution of grain boundaries. The properties of a material are contingent upon interatomic positions, relative masses of the atoms, and interatomic potential functions. γ -TiAl alloys possess the fcc lattice-like $L1_0$ -type structure (Fig. 1c), resulting in a lower geometrical symmetry of the lattice structure due to a special axial ratio of $c/a=1.045$. This leads to a reduced slip coefficient and consequently lower ductility. Specific scratch parameters are detailed in Table 1.

The MD model of polycrystalline γ -TiAl alloy is generated using ATOMOSK software^[26], which is based on the Voronoi crystal orientation rotation algorithm. This algorithm can randomly generate grains and grain boundaries with different orientations^[27]. The polycrystalline lattice is formed by establishing random discrete points and connecting them, and then forming a polycrystalline lattice by connecting the discrete points normal to each other, as shown in Fig. 1d. The

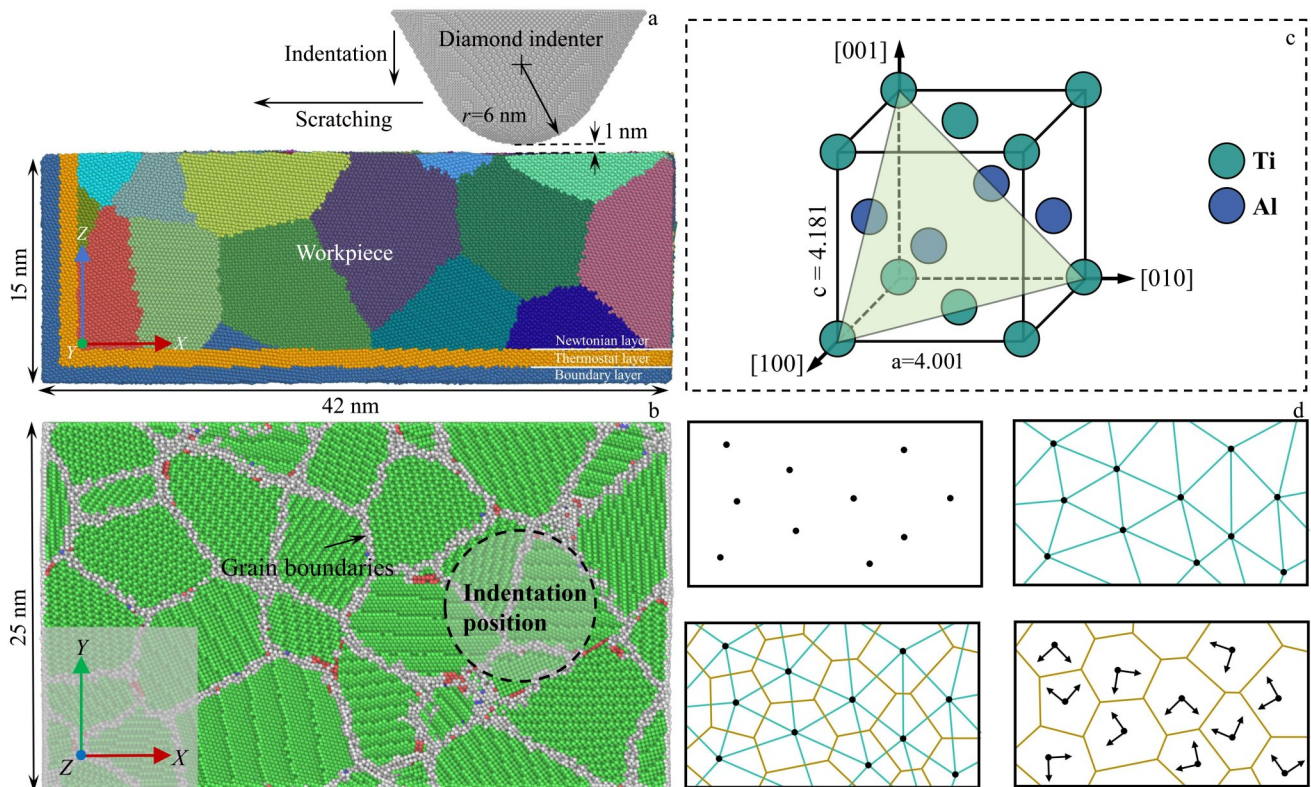


Fig.1 MD model of surface scratches on polycrystalline γ -TiAl alloy (a); top view of grain boundaries distribution for scratch model (b); lattice structure of γ -TiAl alloy (c); schematic diagrams of polycrystalline model construction based on Voronoi algorithm (d)

Table 1 MD simulation parameters for nano-scratching

Simulation parameter	Value
Workpiece dimensions/nm	42×25×15
Tool shape	Cone
Tip angle/(°)	60
Tip radius/nm	6
Scratching depth/nm	2
Scratching length/nm	20
Scratching velocity/m·s ⁻¹	100
Indentation velocity/m·s ⁻¹	100
Initial temperature/K	293
Boundary condition	sps
Potential function	Embedded atom (EAM), Morse
Time step/fs	1

nano-scratch model with different grain sizes can be obtained by changing the number of grains under the same workpiece volume. The values of the grain size (d) and the number of grains (n) in this study are shown in Table 2 and can be calculated using the following Eq. (1)^[28]:

$$\sigma_{vm}(i) = \frac{1}{\sqrt{2}} \left\{ \left[\sigma_{xx}(i) - \sigma_{yy}(i) \right]^2 + \left[\sigma_{yy}(i) - \sigma_{zz}(i) \right]^2 + \left[\sigma_{zz}(i) - \sigma_{xx}(i) \right]^2 + 6 \left[\sigma_{xy}(i)^2 + \sigma_{yz}(i)^2 + \sigma_{zx}(i)^2 \right] \right\}^{\frac{1}{2}} \quad (2)$$

$$\sigma_{hy} = \frac{1}{3} (\sigma_{xx} + \sigma_{yy} + \sigma_{zz}) \quad (3)$$

where σ_{vm} represents the VM stress and σ_{hy} represents the HY stress; i denotes the atomic number; σ_{xy} , σ_{xz} , and σ_{yz} represent the stress components of the atoms in the three orthogonal planes; σ_{xx} , σ_{yy} , and σ_{zz} denote the stress components of the atoms in the three orthogonal directions.

2.2 Potential function

The intermolecular potential function primarily describes the relationship between energy and coordinates in MD modeling. In this study, the EAM potential function was utilized to simulate the interaction of Al atoms and Ti atoms, employing the following atomic energy expressions^[30]:

$$E = \sum_i F_i(\rho_i) + \frac{1}{2} \sum_{j \neq i} \varphi_{ij}(r_{ij}) \quad (4)$$

where F_i represents the density of the atomic electron cloud, ρ_i denotes the embedding energy function, φ_{ij} indicates the interaction function between atoms i and j , and r_{ij} signifies the distance between atoms i and j .

The Morse potential function was utilized to model the interactions between C atoms, and Ti and Al atoms at the nanoscale, using the following theoretical expressions:

$$\varphi(r_{ij}) = E \left[e^{-2\alpha(r_{ij} - r_0)} - 2e^{-\alpha(r_{ij} - r_0)} \right] \quad (5)$$

where E denotes the cohesion energy between atoms i and j , α represents the elasticity coefficient, r_0 indicates the equilibrium distance between atoms i and j , and r_{ij} signifies the instantaneous distance between atoms i and j . The parameters of the Morse potential function are shown in Table 3^[31].

Table 2 Average grain size with different grain numbers

n	9	36	144	576
d_{ave}/nm	14.95	9.41	5.93	3.73

$$n = \frac{6V}{\pi d_{ave}^3} \quad (1)$$

where V represents the volume of the workpiece, d_{ave} denotes the average grain size, and n denotes the number of grains. Additionally, a single crystal model was included as a control group, with the scratch direction of (001) [100].

The simulation results present von Mises (VM) stress analysis to characterize the plastic deformation of the material. VM stress is a yield criterion based on the fourth strength theory, the value of which is based on the shear strain energy as an equivalent force, and the material begins to yield and deform plastically when the stress components in its three directions reach a certain value, i. e., when the elastic deformation energy of the unit cell reaches a certain level. Additionally, the hydrostatic compressive (HY) stress is incorporated to represent the state and distribution of tensile and compressive stresses in the material during the scratching process. The computational expressions for VM and HY stress are provided below^[29]:

3 Results and Discussion

3.1 Effect of grain size on mechanical properties

As depicted in Fig. 2a, illustrating the variation in total energy of γ -TiAl alloy substrate with different grain sizes after a relaxation period of 100 ps, the alteration in total energy of substrate is predominantly influenced by changes in surface energy during the stabilization phase of atomic dynamics, due to the presence of size effects at the nanoscale. It is found that the energy steady state is reached in each case before the scratch starts and the total energy of the substrate increases as the grain size decreases, with the energy of the single-crystal substrate being close to that of the substrate with a grain size of 3.73 nm. This is partly attributed to the increase in the number of grains as the grain size decreases, and the increase in the number of grain boundaries on the surface of substrate. These boundaries consist of a large number of disordered amorphous atoms between grains, which occurs as a result of decreasing grain size at a constant volume of substrate. The difference in the number of amorphous atoms leads to variations in total energy due to higher potential energy presence. Additionally, different crystal orientations on the surface of substrate also contribute to differences in surface energy^[32].

Table 3 Parameters of Morse potential function

Parameter	E/eV	α/nm^{-1}	r_0/nm
Ti-C	0.9820	22.830	0.18920
Al-C	0.2800	27.800	0.22000

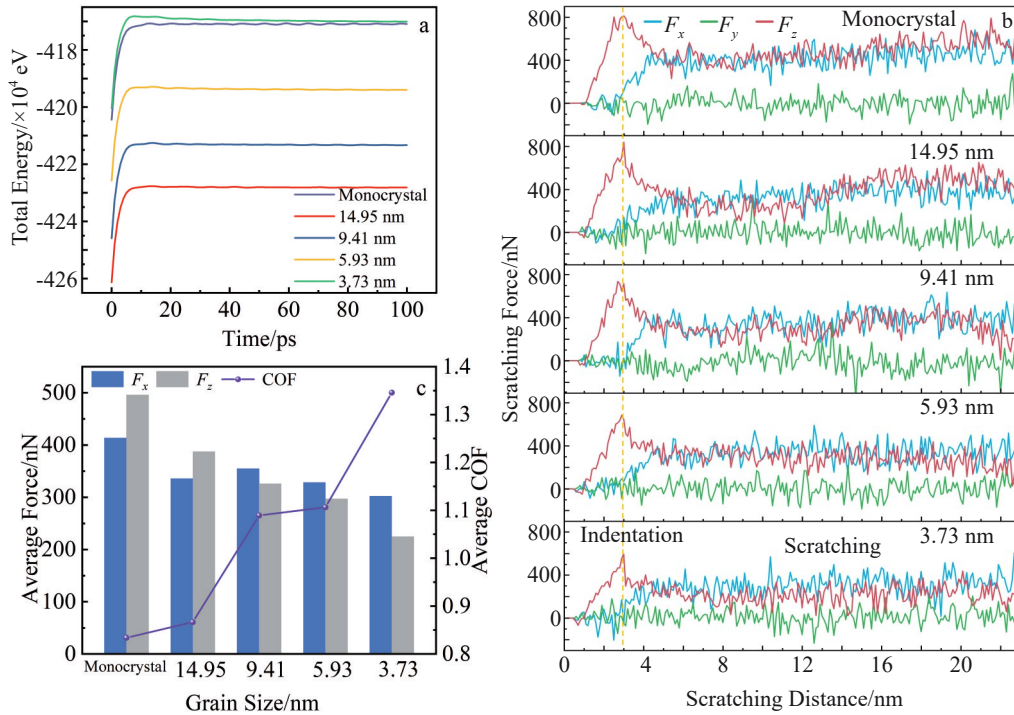


Fig.2 Total energy change during relaxation (a), variation curves of scratch force with distance (b), and average friction force and average COF for different grain sizes (c)

The magnitude of the scratch force during the scratching process is a crucial parameter for evaluating the mechanical response of the material. Fig. 2b presents the instantaneous scratch force variation curves for different grain sizes, defining the combined force along the x -direction as the friction force F_x , the combined force along the z -direction as the normal force F_z , and F_y denoting the force on both sides of the tool in the y -direction. The entire machining process is bounded by a yellow dashed line, with two regions before and after indicating the indentation stage and scratching stage, respectively. It is observed that there are fluctuations in instantaneous scratch force with distance, which are closely related to material removal mode and dislocation activity. During the indentation stage, F_z increases dramatically. When it enters the scratching stage, F_z begins to decrease due to a shift in the force position of the indenter tip, while F_x remains stable after increasing rapidly. Once the tip of the indenter moved about 5 nm, the scratch stabilization stage was entered, and both F_z and F_x fluctuated up and down around a stable value. In particular, at an average grain size of 14.95 nm, F_z showed a tendency to decrease and then increase within a scratch distance between 3–16 nm. This phenomenon is attributed to the large ratio of grain size to the geometry of the indenter tip at this time, as well as variability in elastic modulus affecting changes in F_z , when scratching across grains with different crystal orientations and grain boundaries. The difference in orientation between neighboring grains directly affects the surface profile on both sides of grain boundaries, thus influencing machined surface roughness^[28].

Additionally, the periodic boundary conditions set in the y -direction within this simulation system along with the special geometry of the tool and constant loading pattern result in F_y always fluctuating around 0 throughout the process.

To further clarify the impact of grain size on scratching performance, the average values of friction force F_x and normal force F_z , as well as the average COF during the scratching process, are statistically presented in Fig. 2c. The COF is defined as the ratio of the friction force on the indenter to the normal force, so COF is heavily correlated with F_x and F_z ^[33]. It was observed that F_z decreases with decreasing grain size. However, when scratches on the surface of a single crystal are not considered, F_x is maximum at a grain size of 9.41 nm and then decreases with decreasing grain size, showing an overall trend of increasing and then decreasing. This finding is consistent with a critical size of 9.96 nm for γ -TiAl alloys obtained from Ref. [15]. This trend is attributed to the inverse H-P effect that occurs when the grain is refined to a critical size, due to different plastic deformation mechanisms at different grain sizes, which are mainly controlled by dislocation-induced shear deformation when larger than the critical grain size, and by grain boundaries when smaller than the critical grain size^[34].

In addition, it was observed that COF increases with decreasing grain size, implying that the indenter tip slides more easily on smaller grain-size surfaces. This is because when the grain size is smaller, the number of amorphous atoms forming grain boundaries between neighboring grains increases, and the bonding strength between the atoms

decreases, which softens the material and exhibits better tribological properties. These findings align with previous studies by Peng et al.^[35] on friction experiments involving metals of varying grain sizes and Gao et al.^[36] on scratches observed on single-crystal Fe surfaces.

3.2 Effect of grain size on scratch morphology

Fig. 3a represents the surface scratch morphologies of γ -TiAl alloy with different grain sizes. When the tip of the indenter scratches the surface of the material, it normally goes through three stages, which are adhesion, ploughing, and cutting^[37]. In the pre-scratching stage, no stable abrasive chips are formed, only elastic-plastic deformation occurs, the material flows further toward the subsurface, and a modest number of atoms are gathered on the front side of the tool. With the increase in the scratching distance, the atoms on the front side of the tool gradually accumulate, and when the accumulation reaches a certain threshold, the atoms are plowed by the edge of the conical tool to the sides of the nano-groove to form pile-ups. Subsequently, the nano-groove is initially formed and enters a stable material removal phase. In all cases, the pile-up is mainly concentrated on the frontal side of the tool as the scratch distance increases, and the pile-up structure of the atoms is found to exhibit significant differences. Surface pile-up was also symmetrical in the case of single crystals and at a grain size of 3.73 nm, with lateral pile-up occurring around the time of scratching up to 10 nm. In all other cases, irregular pile-up and side-flow on both sides

of the grooves appeared, and the moment of appearance of the pile-up on both sides was not regular, which was due to different crystal orientations of the grains on the surface of the workpiece, and the crystal orientation significantly affected the pile-up of the scratches. Furthermore, Shugurov et al.^[38] similarly found that grain orientation had a greater effect on the formation of the scratch morphology of pile-up in the scratching test and MD of polycrystalline Ti.

In addition, when the grain size decreases to 3.73 nm, the number of grain boundaries increases, and the plastic deformation of the material is mainly dominated by grain boundary deformation. The material exhibits isotropy as a whole, which makes the surface build-up of the material more regular and controllable. A similar situation is observed for single crystals, which leads to symmetric surface pile-up due to the scratch direction set to $(001)[\bar{1}00]$, and the extremely regular and symmetric atomic lattice structure on both sides of the scratch path.

To further assess the surface pile-up characteristics of γ -TiAl alloys under the influence of grain size, Fig. 3b quantifies the number of removed atoms at various grain sizes during scratching up to a depth of 20 nm. Atoms with spatial positions exceeding 15 nm in the z -direction are considered as removed atoms. It is observed that during the initial stage of scratching (tool travel distance of 0–1.5 nm), only elastic deformation occurs without significant atom removal. Subsequently, there is a remarkable increase in the number of

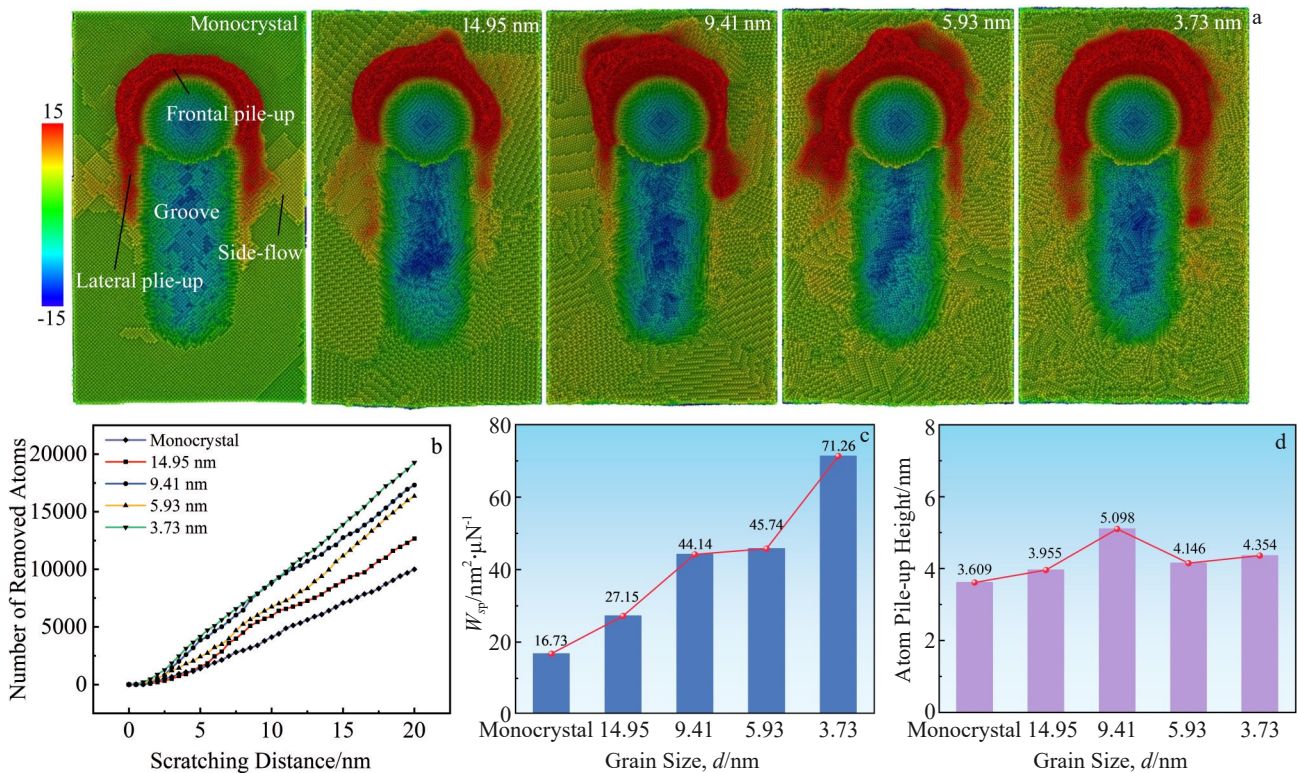


Fig.3 Surface scratch morphologies of γ -TiAl alloy at different grain sizes with blue to red color indicating low to high atom positions (a); number change of removed atoms with scratching distance (b); specific wear rate W_{sp} at different grain sizes for scratches up to 20 nm (c); maximum height of atom pile-up at different grain sizes (d)

removed atoms for each case as the scratching distance progresses. It can be distinctly observed that the rate of removed atoms is the fastest as the grain size is refined, with the most removed atoms up to 20 nm. To better discuss the contribution of pile-up atoms to the friction effect, it is common to express the wear of the material by utilizing its specific wear rate, W_{sp} , as shown in the following Eq. (6)^[39]:

$$W_{sp} = \frac{V_T}{F_z L} \quad (6)$$

where V_T represents the wear volume of atomics, with Al and Ti denoting the average atomic volumes of 16.6×10^{-3} and $17.67 \times 10^{-3} \text{ nm}^3$, respectively. F_z refers to the normal force; L indicates the scratch length.

As shown in Fig. 3c, the W_{sp} at different grain sizes is counted. The decrease in grain size leads to an increase in W_{sp} . This observation implies that refining the grain can exert a significant influence on the removal rate of material, with a more pronounced friction effect on the material surface. Furthermore, as depicted in Fig. 3d, this study quantifies the maximum height of surface pile-up for the material. It is observed that the stacking height initially increases with decreasing grain size. However, a sudden decrease occurs at a grain size of 9.41 nm, followed by a slight increase thereafter. This behavior can be attributed to both the random crystallographic orientation of grains and the reduction in grain strength below the critical size due to the inverse H-P effect. As the flow of atoms during the scratching process exists in a stagnant region, atoms above the stagnant region form chips, while atoms below the stagnant region flow downward to form the machined surface^[40]. As the grain size is refined, the gradually increasing material strength affects the material flow, making it difficult for the atoms to flow inside the substrate through the action of the indenter tip, preferring to form a pile up on the front side of the tool as well as on the sides of the grooves, which results in a higher pile-up height. However, as the grain size exceeds the threshold, the increased grain boundary activity induces stress relaxation, and large-scale slip channels are formed inside the grain boundary, leading to a tendency for atoms to flow inside the substrate, resulting in a lower pile-up height.

During nano-scratching, due to the stress concentration at the tip of the indenter, atoms in strong compression tend to recover to an equilibrium position to reduce the residual stress after scratching. This is manifested by the expansion of atoms in the groove above the scratch depth after the scratch, and this elastic recovery has a great impact on the surface morphology of the processed surface. As shown in Fig. 4, the number of elastic recovery atoms at different grain sizes was counted^[41], and the atoms undergoing elastic recovery were colored in white. It can be observed that the elastic recovery mainly occurs at the indentation location, and the number of elastically recovered atoms is found to firstly decrease and then increase as the grain size decreases, and then slightly decrease again when the grain size is less than 5.96 nm. It is found that a single crystal has the strongest elastic recovery in all the cases of this research and the weakest elastic recovery

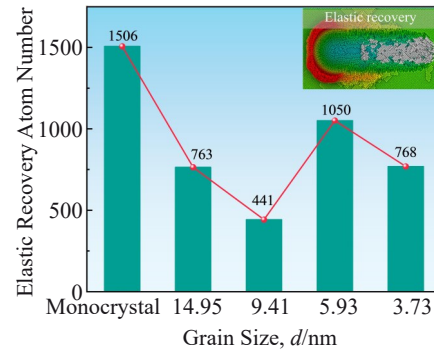


Fig.4 Number of elastic recovery atoms on machined surface when scratch reaches 20 nm

of the material is found at a grain size of 9.41 nm. In this case, the crystallographic orientation of the grains has a great influence on the scratch morphology as well as the trench atomic elastic recovery. It can be observed from the atomic height coloring in Fig. 3a that the deeper blue area inside the groove implies a deeper groove depth, which is due to the grains on the unprocessed surface being in a soft orientation. Furthermore, when the tool scratches through tough oriented grains, the occurrence of elastic recovery or grain rotation as well as grain boundaries can result in atoms higher than the scratch depth^[42].

3.3 Effect of grain size on microscopic defects

To further discuss the plastic deformation mechanism and microscopic defect distribution under the influence of grain size, the atomic lattice structure and dislocation types during the scratching process were identified and visualized by the CNA algorithm and dislocation extraction analysis (DXA) algorithm in the OVITO software^[43]. The defect distribution under the influence of different grain sizes is shown in Fig. 5a–5e. It can be observed that as the grain size becomes smaller, there are different removal mechanisms for the material. At larger grain sizes, dislocation-induced shear deformation dominates, as shown in region I of Fig. 5b, and dislocation motion up to grain boundaries is found to be absorbed, indicating that the grain boundaries create an impediment to the motion of the layer dislocations, as shown in region II of Fig. 5b. With the grain size refinement to 5.93 nm, the tool geometry is comparable to the grain size, and the phenomenon of grain boundary sliding appears in region III of Fig. 5d. The workpiece is squeezed by the tool, and the slip channel at the grain boundary on the front side of the tool is activated. The grains slip along the grain boundary toward the substrate surface. In addition, twin boundaries^[44] emitted from the grain boundaries (consisting of one layer of HCP atoms) were found to exist in one grain, as shown in region IV of Fig. 5d. Furthermore, extrinsic stacking fault characterized by two layers of hcp atoms sandwiching a layer of fcc atoms and intrinsic stacking fault consisting of two adjacent layers hcp atoms were also observed. At the same time, a localized machined surface consisting of G3 grains in Fig. 5d was observed at the bottom of the groove above the normal scratch

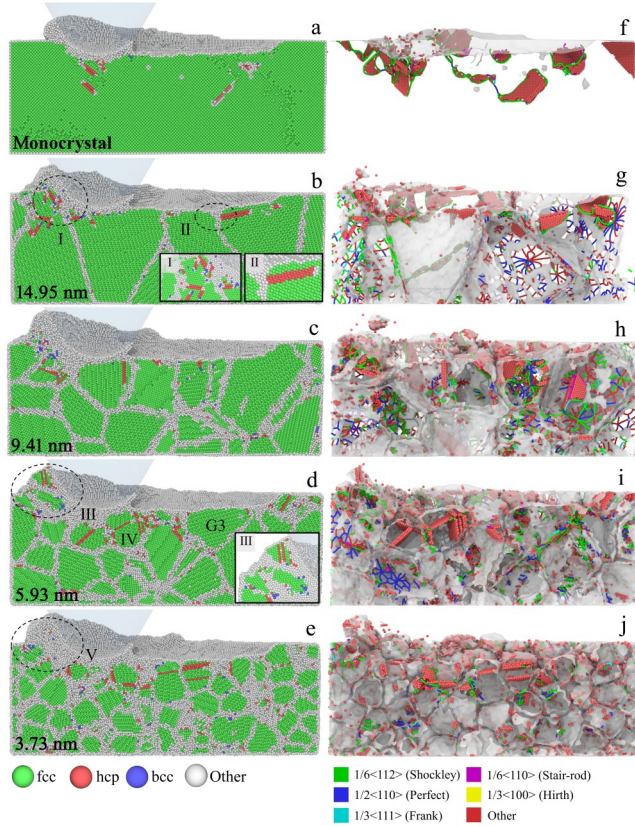


Fig.5 Microscopic defect distribution by CAN analysis (a–e) and DXA analysis (f–j) for different grain sizes: (a, f) monocrystal; (b, g) 14.95 nm; (c, h) 9.41 nm; (d, i) 5.93 nm; (e, j) 3.73 nm

depth, indicating that the grain orientation of this grain is hard-oriented and susceptible to elastic recovery, which corresponds to the larger number of elastic recovery atoms at a grain size of 5.93 nm in Fig.4. When the grain size was 3.73 nm, as shown in Fig. 5e, a large number of disordered amorphous atoms (region V) were gathered in the front side of the tool. This indicates that at this time, the material removal mode for the tool's extrusion, ploughing action as the dominant grain orientation and grain boundaries for the formation of pile-ups and abrasive debris weakened the influence of the surface pile-up, manifested as a more regular and symmetrical surface morphology of the pile-up in Fig.3a.

Fig. 5f–5j represents the DXA analysis from scratch to maximum distance, and the fcc, bcc, and additional atoms are hidden to observe the distribution of dislocations more precisely. Compared with single crystals, there are a large number of perfect dislocations and stair-rod dislocations in polycrystalline. And the dislocations react with each other to form a large number of dislocation networks as well as dislocation entanglements at the grain boundaries, which is in agreement with the conclusions obtained by Xue et al^[45] in their experiment and simulation studies on the plastic deformation of AZ31 magnesium alloy. They indicated that there are higher energies and higher hardness at the grain boundaries. The presence of intact and tall Shockley dislocations in single crystals indicates active shear

deformation behavior within the single crystal substrate. Whereas polycrystalline γ -TiAl Alloy have shorter Shockley dislocations due to the presence of grain boundaries, resulting in the suppression of dislocation-induced shear that occurs in the grains. It was found that the total length of grain boundaries increased as the grain size decreased to 3.73 nm. However, the grain boundaries length of neighboring grains decreased. The potential energy of a tiny number of disordered and active amorphous atoms in the grain boundaries failed to reach the energy threshold required for dislocation entanglement formation, which suppressed the formation of dislocation networks. A similar phenomenon was found by Niu et al^[46] in MD simulations on the mechanical properties of polycrystalline Ti. In addition, it was found that the defects were mainly concentrated within the grains and grain boundaries at the scratch paths and surfaces. There was randomness in the expansion of stacking lamination faults inside the workpiece due to the randomness of grain orientation and non-uniformity of grain size. Whereas, smaller subsurface depths were found at a grain size of 3.73 nm as the density of grain boundaries increased, suggesting that grain refinement suppressed the depth of subsurface damage under certain conditions.

The hcp atoms are the most dominant type of atomic phase transition, which indicates the initiation of the slip system inside the γ -TiAl alloy^[47]. In addition, the number of amorphous atoms represents grain boundary atoms; it on the one hand verifies the previous increase in grain boundaries as the grains become smaller, and on the other hand indicates the degree of amorphization caused by the tool-squeezing action after scratching. To further assess defect evolution and plastic deformation of materials influenced by grain size, the changes in phase transition atom count and dislocation length during nano-scratching were quantified.

Fig.6a illustrates the variation in the number of other atoms before and after scratching. Before scratching, it was observed that the number of grain boundaries increased as the grain size decreased, leading to an increase in the number of amorphous atoms. Subsequently, after completing the scratching process, there was a noticeable increase in the number of amorphous atoms due to pile-up generation. In Fig.6b, the number of hcp atoms before and after scratching is presented. It was noted that as the grain size became finer, the number of hcp atoms increased due to the elevated energy-induced lattice reorganization at additional grain boundaries, which was consistent with observations from Fig.5j. The large increase in the number of hcp atom at the end of scratching indicated that the extension of stacking lattice dislocations induced strong plastic deformation inside the substrate. Fig.6c displays the curve of the number of hcp atoms with increasing scratch distance. A comparison with Fig. 6b reveals that plastic deformation within the substrate is more pronounced at a grain size of 5.93 nm during the scratching process. In addition, monocrystals and grains with a size of 14.94 and 5.93 nm show a faster rate of change in the number of hcp atoms during the indentation stage. On the one hand, that is

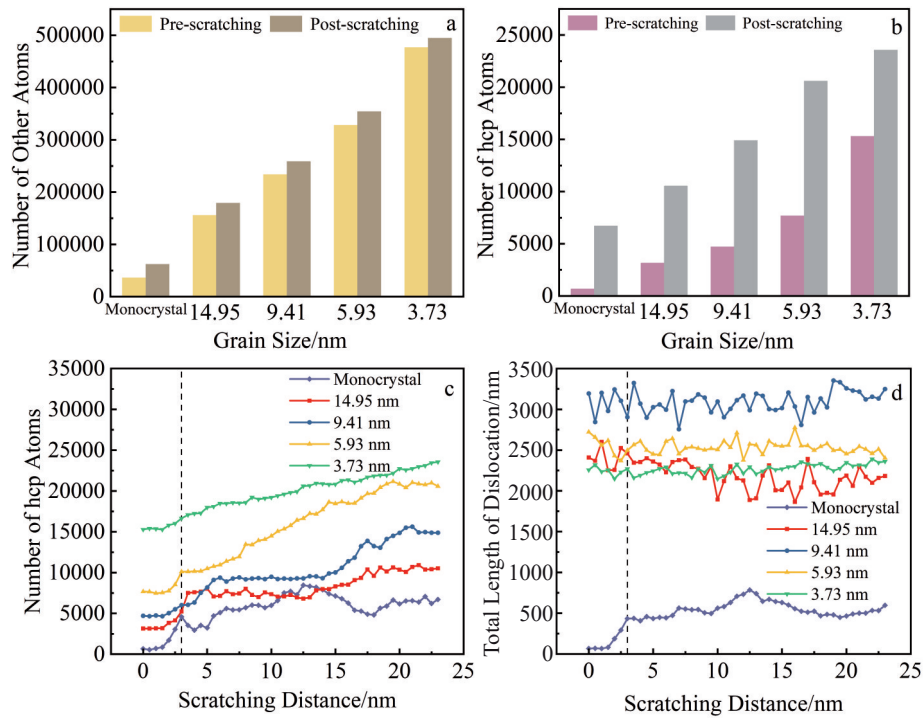


Fig.6 Variation in number of other atoms (a) and hcp atoms (b) before and after scratching; variation curves of hcp atoms (c) and total dislocation length (d) with scratching distance

due to the absence of the influence of grain boundaries in the single crystal, where the initiation of the slip system is not hindered. On the other hand, due to the effect of random grain orientation in polycrystalline, the indentation may act on the harder grains. In particular, at a grain size of 3.37 nm, the rate of increase in atomic number during both the indentation and scratching phases remains consistent. This can be attributed primarily to the softening effect induced by an increased number of grain boundaries, where the abrupt change in stress has minimal impact on atomic phase transition. Instead, it is predominantly the thermal-force coupling resulting from friction that triggers stacking fault nucleation.

The variation curves of total dislocation length during the scratching process are depicted in Fig. 6d, which effectively represent the plastic deformation of the material. It can be observed that, with grain refinement, the dislocation length of the initial workpiece after relaxation exhibits an increasing and then decreasing trend. This additionally confirms the existence of a critical grain size (9.41 nm) under the influence of the inverse H-P effect, at which there is maximum dislocation length. When grain size is smaller than this critical value, as shown in Fig. 5f–5j, the dislocation length decreases. The curves for each case exhibit varying degrees of fluctuation as the scratch progresses. Notably, larger grain size results in drastic changes in dislocation length, while finer grains tend to flatten the dislocation curves. This observation suggests that larger grains provide ample space for dislocation slip and facilitate the nucleation, extension, interaction, and annihilation of dislocations through a more extensive network distribution, leading to pronounced shear deformation.

Conversely, smaller grains with an increased presence of grain boundary lattices exert an inhibitory effect on dislocation budding and expansion. Furthermore, it is noteworthy that the monocrystal experiences a significant increase in dislocation length towards the end of the scratch.

3.4 Effect of grain size on temperature

The accumulation of temperature during the scratching process leads to an increase in atomic kinetic energy, thereby influencing the activation and motion of dislocations as well as the phase transition of atoms. Fig. 7a depicts the schematic diagram illustrating the temperature distribution at various grain sizes for scratching up to 20 nm, with temperature changes occurring within the Newtonian layer. Temperature is primarily concentrated around the abrasive chips and at the tip of the indenter. As the scratching distance increases, frictional interactions with wear atoms result in enhanced atomic kinetic energy, causing total energy diffusion in a thermal gradient centered on the tool towards the interior of the workpiece. Different grain sizes reveals that the decrease in grain size extends the range of temperature diffusion, with single crystals exhibiting minimal diffusion. To better illustrate the influence of grain size on temperature, Fig. 7b statistically presents the temperature distribution of abrasive chip atoms (indicated by the black dashed box in Fig. 7a). It is observed that the chip temperature increases with decreasing grain size, excluding monocrystal, and exhibits a slight decrease at a grain size of 5.93 nm. The temperature of abrasive chip atoms is found to be correlated with both their pile-up height and atom removal rate. Notably, the highest abrasive chip temperature is observed when the grain size is 3.73 nm.

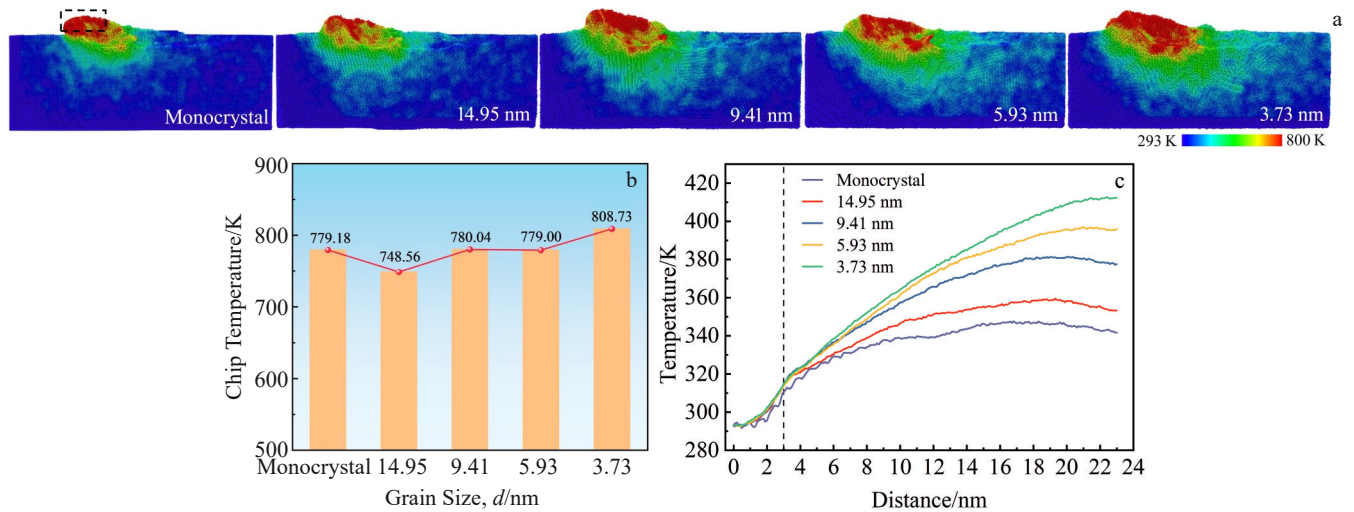


Fig.7 Temperature distribution (a), abrasive chip temperature (b), and temperature change of Newton layer with scratch distance under different grain sizes (c)

Fig.7c illustrates the instantaneous variation curves of the temperature for the Newtonian layer with increasing scratch distance. It is observed that the rate of temperature increase is higher at the indentation stage (0–3 nm). This phenomenon can be attributed to the absence of abrasive chip generation during indentation, making it difficult for the temperature to dissipate. As the tool enters the scratching stage, there is a gradual accumulation of atoms and an increased friction effect between the tool and atoms, resulting in a continuous rise in temperature. However, it was noted that the rise rate of temperature slightly decreased due to some heat being carried away by abrasive chips. Furthermore, it was found that as grain size decreases, the curve becomes smoother, and there is more drastic temperature fluctuation in both indentation and scratching stages within monocrystal Newtonian layers. This behavior can be attributed to dislocation motion dominating plastic deformation without any blockage from grain boundaries in single crystals. The larger range of motion on slip surfaces leads to more violent plastic deformation dominated by dislocation motion, which causes energy fluctuations and leads to large temperature fluctuations. In addition, the temperature of the Newton layer at 20 nm tends to decrease due to the partial absorption of heat by the tool as it approaches the thermostat layer. This is consistent with the temperature distribution shown in Fig. 7a, indicating that smaller grain size results in higher Newton layer temperature. This can be attributed to both an increase in friction effect (as seen from the increase in COF in Fig.2c) and grain refinement which leads to a greater distribution of amorphous atoms at grain boundaries. The weak bonding between these amorphous atoms results in stronger kinetic energy for single atoms, making them more active when subjected to external forces and promoting the propagation of heat along grain boundaries.

3.5 Effect of grain size on stress distribution

The stress distributions of VM and HY during nano-

scratching on the surface of γ -TiAl alloy under different grain sizes are statistically presented in Fig. 8, with a scratch distance of 16 nm. An evident stress concentration is observed in the contact region between the indenter tip and the material, as well as in the abrasive chips and the front and lower part of the tool. To further elucidate the impact of grain size on VM stress concentration, the average VM stress was quantified within the extreme stress region around the indenter in Fig.8a–8e, as indicated by the range delineated by white dashed lines. It has been observed that the average VM stress decreases as the grain size decreases. The largest average VM stress of 32.973 GPa is found for monocrystals, while the smallest is 30.537 GPa at the grain size of 3.73 nm. This gradient change can be attributed to two main factors. Firstly, an increase in surface grain boundaries allows for an increase in wear rate and thermal effects caused by the scratching process (Fig.3c), leading to softening of the stacked material on the front side of the tool. Secondly, due to the lattice distortion of the disordered atoms in the unprocessed front grain boundaries, the gap between the atoms is large, and the overall structure is loose, which reduces the stress transfer barrier on the grain boundaries. With the interaction between the tool and the material, the plastic deformation degree of the grain boundary is greater than that of the grain interior, which shows that there is a large VM stress at the grain boundary inside the substrate. As the grain size decreases, the increased grain boundary area results in a rapid release of stresses, leading to a larger range of VM stress spreading in small grain sizes and a higher concentrated stress at the indenter tip in large grain sizes. This phenomenon is consistent with previous findings^[48]. From Fig.8f–8j, it can be distinctly observed that HY stress is primarily concentrated at the front and lower part of the tool as well as in the grain. Notably, as the grain size decreases, the effect of HY stress diminishes. The combination of these analyses suggests that this phenomenon can be attributed to the absorbing and hindering effect of grain

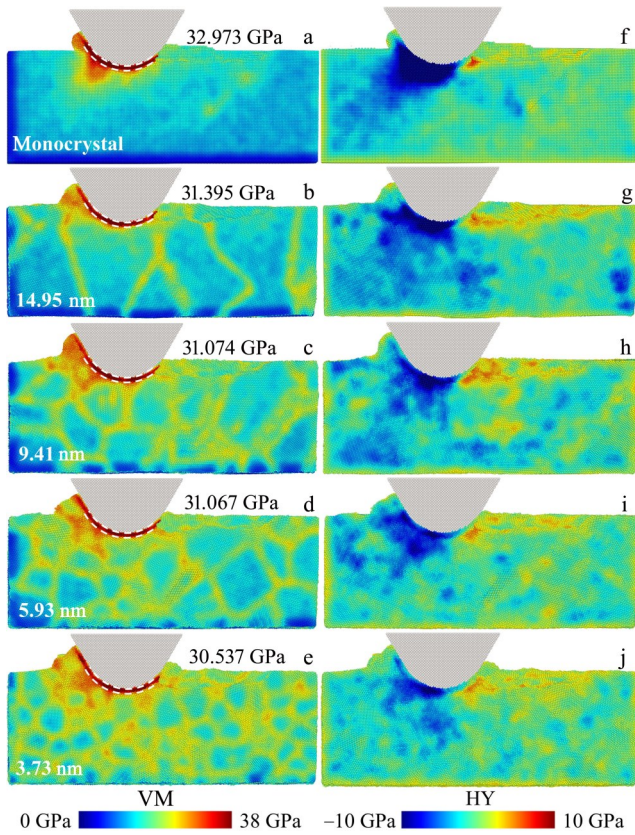


Fig.8 VM stress distribution (a–e) and HY stress distribution (f–j) under different grain sizes: (a, f) monocrystal; (b, g) 14.95 nm; (c, h) 9.41 nm; (d, i) 5.93 nm; (e, j) 3.73 nm

boundaries on stress, while also considering that crystal orientation randomness has some influence on the distribution of HY stress. Simultaneously, it is evident that the tensile stress is predominantly concentrated at the rear of the tool and along the scratch path. This phenomenon is attributed to the friction and adhesion effects, which cause the atoms on the machined surface to adhere to the tip of the indenter and move in the direction of the scratches, resulting in a certain amount of tensile stress component. Furthermore, smaller grain sizes exhibit a wider range of residual stresses within the substrate.

4 Conclusions

1) Single crystals demonstrate stronger scratch resistance and favorable tribological properties. When excluding single crystals, the average F_x exhibits a trend of initially increasing and then decreasing as the grain size decreases, while F_z continues to decrease due to the inverse H-P effect. There is a critical grain size of 9.41 nm at which F_x is at its maximum, and the average COF increases with decreasing grain size.

2) The shape of the pile-up on both sides of the scratched surface and the start moment of molding are significantly influenced by grain size and crystal orientation randomness. At a grain size of 3.73 nm, consistent with the single-crystal case, the substrate surface pile-up is also regular and symmetric. The highest stacking height and the smallest

atomic number are observed at a grain size of 9.41 nm. Additionally, both the number of removed atoms and W_{sp} increase due to grain refinement.

3) At larger grain size, dislocation-induced shear deformation as well as grain boundary slip are dominant. The presence of grain boundaries has an impeding effect on the movement of the laminar dislocations. When the grain size is 3.73 nm, the increase in the number of grain boundaries leads to softening of the material surface. During this time, the removal mode is dominated by the extrusion and ploughing action of the tool, resulting in a smaller subsurface depth. As the grain size decreases, there is a gradual flattening of the dislocation length curve with scratch distance, transitioning from drastic to flat.

4) The increased grain boundary area promotes temperature rise and stress release. As the grain size decreases, the temperature distribution range is larger, the abrasive chip temperature and the Newtonian layer temperature tend to increase, and the temperature fluctuation is smoother. The average VM stress in the region of extreme stress concentration decreases due to grain refinement, and the range of HY stress distribution below the front of the tool becomes smaller with the decrease in grain size due to the blocking of grain boundaries and the randomness of grain orientation.

References

- 1 Xia Z W, Shan C W, Zhang M H et al. *Chinese Journal of Aeronautics*[J], 2023, 36(7): 40
- 2 Xu R R, Li M Q, Zhao Y H. *Journal of Alloys and Compounds*[J], 2023, 932: 167611
- 3 Zhang Y, Lee Y J, Chang S et al. *International Journal of Machine Tools and Manufacture*[J], 2022, 174: 103851
- 4 Genc O, Unal R. *Journal of Alloys and Compounds*[J], 2022, 929: 167262
- 5 Hu D. *Intermetallics*[J], 2001, 9(12): 1037
- 6 Kumar S, Pandey V, Chattopadhyay K et al. *Transactions of the Indian Institute of Metals*[J], 2019, 72(3): 789
- 7 Chen R R, Zheng D S, Guo J J et al. *Materials Science and Engineering A*[J], 2016, 653: 23
- 8 Yao J Q, Fan S, Liu X W et al. *Materials Science and Engineering A*[J], 2023, 865: 144630
- 9 Zhang K R, Hu R, Li J G et al. *Materials Letters*[J], 2020, 274: 127940
- 10 Hu H, Fu T, Li C Y et al. *Physical Review B*[J], 2022, 105(2): 024107
- 11 Takeuchi S. *Scripta Materialia*[J], 2001, 44(8): 1483
- 12 Ding J, Tian Y, Wang L S et al. *Computational Materials Science*[J], 2019, 158: 76
- 13 Cao P, Rui Z Y, Fu R et al. *Rare Metal Materials and Engineering*[J], 2021, 50(6): 2052
- 14 Liu S Q, Ding H S, Chen R R et al. *Materials Science and Engineering A*[J], 2021, 823: 141692
- 15 Cao H, Yu Z L, Zhou B C et al. *Vacuum*[J], 2023, 217: 112498

- 16 Chen D J, Wu S Y, He Y Z et al. *The International Journal of Advanced Manufacturing Technology*[J], 2022, 121(3): 1533
- 17 Huang Y H, Zhou Y Q, Li J M et al. *International Journal of Mechanical Sciences*[J], 2022, 235: 107719
- 18 Wang J Q, Yan Y D, Li Z H et al. *International Journal of Machine Tools and Manufacture*[J], 2021, 162: 103701
- 19 Qi Y M, He T W, Xu H M et al. *Journal of Alloys and Compounds*[J], 2021, 871: 159516
- 20 Doan D Q, Fang T H, Chen T H. *International Journal of Mechanical Sciences*[J], 2020, 185: 105865
- 21 Chamani M. *The European Physical Journal Plus*[J], 2024, 139(5): 426
- 22 Xie H C, Ma Z C, Zhao H W et al. *Materials Today Communications*[J], 2022, 30: 103072
- 23 Xu H Z, Cao H, Huang Q Q et al. *Vacuum*[J], 2024, 226: 113192
- 24 Zheng M, Han J F, Qu D F et al. *Physica Scripta*[J], 2024, 99(6): 065001
- 25 Plimpton S. *Journal of Computational Physics*[J], 1995, 117(1): 1
- 26 Hirel P. *Computer Physics Communications*[J], 2015, 197: 212
- 27 Sun H, Béland L K. *Scripta Materialia*[J], 2021, 205: 114183
- 28 Guo Z T, Cao H, Fu R et al. *Modelling and Simulation in Materials Science and Engineering*[J], 2023, 31(6): 065017
- 29 Liu C L, Zhuang Z X, Chen J et al. *Surfaces and Interfaces*[J], 2023, 40: 103126
- 30 Zope R R, Mishin Y. *Physical Review B*[J], 2003, 68(2): 024102
- 31 Girifalco L A, Weizer V G. *Physical Review*[J], 1959, 114(3): 687
- 32 Barwicz T, Cohen G M, Reuter K B et al. *Applied Physics Letters*[J], 2012, 100(9): 093109
- 33 Liu Y J, Chen W H, Qu D F et al. *Vacuum*[J], 2024, 225: 113232
- 34 Cao H, Guo Z T, Feng R C et al. *Journal of Manufacturing Processes*[J], 2023, 102: 169
- 35 Peng L F, Mao M Y, Fu M W et al. *International Journal of Mechanical Sciences*[J], 2016, 117: 197
- 36 Gao Y, Urbassek H M. *Applied Surface Science*[J], 2016, 389: 688
- 37 Zhang L C, Tanaka H. *Wear*[J], 1997, 211(1): 44
- 38 Shugurov A, Panin A, Dmitriev A et al. *Wear*[J], 2018, 408–409: 214
- 39 Zhang J, Deng G Y, Li W Y et al. *Surface and Coatings Technology*[J], 2023, 468: 129772
- 40 Liu B, Xu Z W, Chen C et al. *Applied Surface Science*[J], 2020, 528: 147034
- 41 Liu C L, To S, Sheng X X et al. *Discover Nano*[J], 2023, 18(1): 91
- 42 Zhou Y C, Cao H, Zhou B C et al. *Modelling and Simulation in Materials Science and Engineering*[J], 2024, 32(6): 065005
- 43 Stukowski A. *Modelling and Simulation in Materials Science and Engineering*[J], 2010, 18(1): 015012
- 44 Cao H, Yang W L, Zhou B C et al. *Rare Metal Materials and Engineering*[J], 2023, 52(12): 4073
- 45 Xue C, Gao B, Han T Z et al. *Computational Materials Science*[J], 2024, 231: 112606
- 46 Niu Y, Jia Y J, Lv X et al. *Materials Today Communications*[J], 2024, 40: 109558
- 47 He T J, Yi B Q, Zheng M et al. *Materials Today Communications*[J], 2024, 38: 107965
- 48 Papanikolaou M, Salonitis K. *Applied Surface Science*[J], 2021, 540: 148291

晶粒尺寸对多晶 γ -TiAl合金表面纳米划痕行为影响的分子动力学模拟

曹 卉^{1,2}, 徐汉宗¹, 李海鹏³, 李海燕^{1,2}, 陈 涛⁴, 冯瑞成^{1,2}

(1. 兰州理工大学 机电工程学院, 甘肃 兰州 730050)

(2. 兰州理工大学 有色冶金新装备教育部工程研究中心, 甘肃 兰州 730050)

(3. 云南文山铝业有限公司, 云南 文山 663000)

(4. 常州大学 机械与轨道交通学院, 江苏 常州 213164)

摘要: 基于分子动力学的方法, 从原子尺度研究了不同晶粒尺寸影响下的多晶 γ -TiAl合金表面划痕机理, 分析了划痕过程中的力学特性、划痕形貌、微观缺陷分布以及温度和应力状态。结果表明, 由于逆霍尔佩奇效应的影响, 划痕力、原子回弹数量和堆积高度在临界尺寸为9.41 nm时出现突变。晶界数量的差异以及晶粒的晶粒取向随机性导致划痕表面堆积不同, 其中单晶材料和晶粒尺寸为3.73 nm情况下的表面形貌更加规则。此外, 晶粒尺寸越小, 平均摩擦系数、原子去除数量以及特殊磨损率随之增加, 温度的数值和分布范围更大。由于晶界的阻碍作用, 小尺寸的晶粒有更少的微观缺陷, 并且压头尖端处的平均冯·米塞斯应力和静水压应力随着晶粒尺寸的减小而减小。

关键词: 晶粒尺寸; 纳米划痕; 表面形成; 亚表面缺陷; 多晶 γ -TiAl合金

作者简介: 曹 卉, 女, 1988年生, 博士, 副教授, 兰州理工大学机电工程学院, 甘肃 兰州 730050, 电话: 0931-5135199, E-mail: caoh@lut.edu.cn